Aerospace Science and Technology 32 (2014) 223–234

Contents lists available at ScienceDirect

Aerospace Science and Technology

www.elsevier.com/locate/aescte

On three-dimensional global linear instability analysis of flows with standard aerodynamics codes

F. Gómez [a,c,*], R. Gómez [a], V. Theofilis [b]

[a] INTA Instituto Nacional de Técnica Aeroespacial, Ctra. Ajalvir Km.4 Torrejon de Ardoz, E-28850 Madrid, Spain
[b] School of Aeronautics, Universidad Politécnica de Madrid, Plaza Cardenal Cisneros 3, E-28040 Madrid, Spain
[c] Department of Mechanical and Aerospace Engineering, Monash University, Victoria 3800, Australia

ARTICLE INFO

Article history:
Received 10 May 2013
Received in revised form 8 October 2013
Accepted 15 October 2013
Available online 26 October 2013

Keywords:
Global stability theory
TriGlobal
Matrix-free methods
Lid-driven cavity flows
OpenFOAM

ABSTRACT

The development of a general Jacobian-free approach for the solution of large-scale global linear instability analysis eigenvalue problems by coupling a time-stepping algorithm with industry-standard second-order accurate aerodynamic codes is presented. The three-dimensional lid-driven cavity, a challenging flow in the context of required computational resources and physical complexity, has been chosen for validation. Results in excellent agreement with the literature have been obtained by using the proposed theoretical methodology coupled with the incompressible solver of the open-source toolbox OpenFOAM. The moderate computational resources required for the solution of the TriGlobal eigenvalue problem using this method opens up a new avenue for the performance of instability analysis of flows of engineering relevance.

1. Introduction

Global linear instability analysis theory [76] plays an essential role in the investigation of the sequence of physical mechanisms leading laminar flow in complex, spatially inhomogeneous geometries through transition to turbulence. The theory deals with the temporal and spatial evolution (growth/decay) of small-amplitude perturbations superimposed upon a steady or unsteady laminar base flow. The assumption of asymptotic (long-time) instability leads to a generalized large-scale eigenvalue problem, the challenging numerical solution of which provides the spectrum of linear global modes composed of the modal frequencies and amplification/damping rates. Such numerical solution can be obtained within a matrix-forming or a matrix-free/Jacobian-free framework. The main difference between the two approaches is that matrix-forming strategies provide access to larger subsets of the full spectrum at the cost of large computational memory (RAM memory) while matrix-free methods provides smaller subsets of the full spectrum at the cost of long time integration (CPU time). Both frameworks make use of subspace projection-iterative methods such as the Arnoldi iteration, based on the Krylov-subspaces [67,7], which is one of the most effective techniques to solve the resulting generalized eigenproblem when formation of the full discretized matrix is impractical due to the problem size. The Arnoldi method delivers a window of the eigenspectrum but favors the eigenvalues with the largest modulus, thus a transformation of the spectrum is required in order to introduce an eigenvalue shift towards the interesting part of the spectrum. The shift-invert transformation was first introduced in fluid mechanics in a matrix-forming context by Natarajan and Acrivos [57], while the time-stepping exponential transformation was first developed by Erikson and Rizzi [28] in a Jacobian-free framework. A recent review [76] provides a discussion of the suite of matrix transformation methods used up to the time of writing that article, while recent progress and challenges using these two frameworks has been recently presented by Gómez et al. [34].

Although a large number of studies using the two different frameworks have reported significant insight in instability mechanisms over the last four decades in relatively complex flows with one homogeneous spatial direction, such as attachment lines [62] or open cavities [19], most flows of practical engineering significance still remain unexplored. The principal reason arises from the difficulties associated to the analysis of turbulent flows, an issue not discussed here; the interested reader is referred to the works of Biau et al. [13] and Nichols and Lele [58] amongst others. The second reason for the relatively little attention paid to the analysis of flows of industrial interest is that basic state of most practical flows are three-dimensional depending in an inhomogeneous manner on the three spatial directions, and no assumptions regarding spatial homogeneity can be made; the related analysis context is known as TriGlobal linear stability. Although the single parameter of the instability problem in this situation in incompressible flow is the Reynolds number, the cost of performing a complete

* Corresponding author.
E-mail address: fgomezcarrasco@gmail.com (F. Gómez).

1270-9638/$ – see front matter
http://dx.doi.org/10.1016/j.ast.2013.10.006

Nomenclature

x, y, z	Spatial coordinates	$\mathbf{A}$	Jacobian matrix
$\bar{\mathbf{u}}$	Base flow components	$\mathbf{H}$	Hessenberg matrix
$\mathbf{u}'$	Perturbation components	ϵ	Perturbation magnitude
Re	Reynolds number	ϵ_m	Numerical tolerance
λ	Eigenvalue in the stability analysis	ϵ_o	Initial order of perturbation magnitude
$\hat{\mathbf{u}}$	Eigenvector in the stability analysis	$\varepsilon(t)$	Integration residual at time t
$\mathbf{K}_m$	Krylov subspace	Δt	Time step in temporal integration
m	Krylov subspace dimension	CFL	Courant number
τ	Integration time	N	Number of nodes in one spatial direction

parametric instability analysis can be prohibitively expensive when the matrix discretizing the eigenvalue problem is solved in a dense matrix-forming framework, as inferred from the work of Rodriguez and Theofilis [66], in which a $O(1)$ Tb RAM memory matrix was formed, stored and inverted for the solution of a BiGlobal problem.

Despite the fact that a high-order sparse matrix-forming method has recently been shown to provide $O(10^4)$ speed-up with respect to dense matrix-forming approaches [60], matrix-free methods remain the method of choice for TriGlobal linear instability analysis problem; a case study was provided by Gómez et al. [36,35]. The key advantage of matrix-free time-marching methods, over explicit formation of the Jacobian matrix is that the large-sized matrices describing spatial discretization of global linear instability analysis applications in both two or even more so in three inhomogeneous spatial directions resolved in a coupled manner is never formed. This enables the study of global linear stability problems on small-main-memory machines at the expense of long-time integrations. A rather complete discussion of time-stepping approaches for global linear instability has recently been presented by Barkley, Blackburn and Sherwin [11]. The first successful time-stepping methodology by Erikson and Rizzi [28] introduced a numerical differentiation of the DNS used with a temporal polynomial approximation. In that work, finite differences were used in order to study an inviscid incompressible flow over a NACA airfoil. Chiba [22] improved the Erikson and Rizzi approach by introducing a temporal exponential transformation using a full Navier–Stokes equations solver. Following Chiba's method, Tezuka and Suzuki [71,72] successfully solved the first TriGlobal problem ever. In parallel, Edwards et al. [27] developed a time-stepping methodology in conjunction with the linearized Navier–Stokes equations, which has been successfully used and popularized by Barkley et al. [10], Tuckerman et al. [79] and many others. Although these previously mentioned algorithms are able to provide only a part of the spectrum, recent matrix-free algorithms can provide access to the full spectrum using time-stepping approaches, e.g. Bagheri et al. [8] and elsewhere [54,61].

Despite these new capabilities for global stability analysis that recent sparse matrix-forming and matrix-free algorithms offer, only a number of canonical configurations with three inhomogeneous spatial directions have been analyzed with respect to their linear instability; to the best of the knowledge of the authors, these are the above-mentioned spheroid [72], an incompressible jet in a cross flow [9], sphere [59], and the three-dimensional, lateral-wall-bounded lid-driven cavity [32,53,30,35]. This lack of TriGlobal analyses in the literature can be attributed to the fact that the time-stepping matrix-free methodology requires a three-dimensional Direct Numerical Simulation (DNS) solver and the development and validation of a three-dimensional DNS capable of handling different geometries is non-trivial.

The goal of the present work is to present an algorithm for TriGlobal modal linear instability analysis that can overcome the excessive computational requirements of the matrix-forming techniques and the necessity of developing a three-dimensional direct numerical simulation solver for the specific task. This is accomplished by linking matrix-free/Jacobian-free instability algorithms with existing general purpose aerodynamic codes, the latter run in direct numerical simulation mode. Moreover, the necessity of flexibility and ability to handle complex geometries makes second-order standard aerodynamic codes the first candidate to be examined regarding their suitability for TriGlobal instability analysis. Although no work is known to date that deals with the numerical solution of large-scale TriGlobal eigenvalue problems using standard aerodynamic codes, leaving most problems of practical engineering significance still unexplored, second-order methods have been already successfully used in global linear instability theory both for the solution of the BiGlobal [25,56,43,4,5] and that of the TriGlobal linear EVP [32]. High-order accurate spectral element methods [45,15,77] or even finite elements [37,39] may provide a better convergence rate for a given resolution than second-order finite volumes methods while maintaining geometry flexibility, however the open-source code OpenFOAM code based on second-order finite-volume spatial discretization has been chosen for this work because of its flexibility, ease of performing source-code modifications and the ability this code offers to study different flow regimes in future research.

The three-dimensional, lateral-wall-bounded lid-driven cavity was chosen as a demonstration problem for TriGlobal linear instability analysis, since it permits examining two different aspects: physical complexity and computational efficiency. In addition, the non-unity aspect ratio configuration of this cavity flow, though well-studied from an experimental and a three-dimensional DNS point of view, has never been addressed as regards its TriGlobal linear instability.

From the point of view of physical complexity, the accurate description of the fully three-dimensional lid-driven cavity flow still remains inconclusive in many aspects, as stated in the recent work by Feldman & Gelfgat [30], although the analysis of the two-dimensional counterpart of the lid-driven cavity flow has become a benchmark problem in fluid mechanics and has been extensively reviewed [70,29,18].

The main reason for this lack of understanding is that the three-dimensional lid-driven cavity flow, as found experimentally by Koseff and Street [49,50] and numerically by Iwatsu et al. [42,41], presents a far more complicated structure that cannot be directly compared to the corresponding two-dimensional flow. The most important three-dimensional flow features are the Taylor–Görtler-Like (TGL) vortices [49,69] and corner eddies or end-wall vortices (EWV) [20,63] in the flow field. Fig. 1 shows schematically the geometry and the rest of flow features: primary eddy (PE), downstream secondary eddy (DSE), upstream secondary eddy (USE) and upstream upper eddy (UUE). Aidun et al. [1] performed lid-driven cavity experimental visualizations, presenting an excellent qualitative description of the state diagram of TGL structures and demonstrated the existence of different branches of n-cell

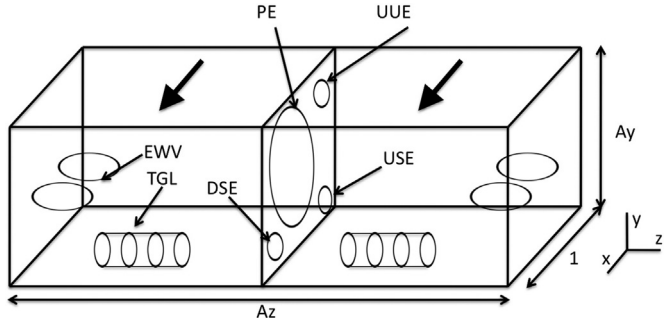

Fig. 1. Geometrical description of the problem and main flow features.

TGL structure. They observed that stability is lost through growth of a steady primary mode with a one-cell pattern and that the flow becomes oscillatory because pf the subsequent competition of the steady modes with the remaining rest of n-cell TGL branches. Guermond et al. [40] carried out comparisons between numerical and experimental start-up flows in lid-driven cavities of aspect ratio $1:1:2$. In agreement to Aidun et al. [1] and Migeon [55], the time evolution of the perturbations showed several TGL structures even at $Re = 1000$. These observations indicate that the stable eigenfunctions of the flow may be related with the TGL structures. In addition, Kim and Moin [47] linked the existence of perturbations with the formation of TGL vortices in their numerical work. Along the same line of qualitative association of linear flow perturbations and TGL vortices, Koseff and Street [49,50] also suggested that most of the velocity fluctuation in the lid-driven cavity at low Reynolds number are caused by the TGL vortices. The above qualitative explanations provide motivation for validating the present methodology with the three-dimensional lid-driven cavity.

Linear stability analysis in the case of periodic boundary conditions, corresponding to a two-dimensional base flow imposing a third homogeneous direction, was first studied by Ramanan and Homsy [64] and later by Ding and Kawahara [26]. Correct critical Reynolds number for different wave number were given by Theofilis et al. [73,78] and Albensoeder et al. [6] among other works. The most unstable eigenvector appears with a wave number of $\beta \sim 15.3$ at a critical Reynolds number $Re_{cr} \sim 783$. Following this methodology, other wall-bounded cavities with one homogeneous spatial direction have been also studied, such as swirling [14], triangular [38] or double-sided [24] lid-driven cavities.

Regarding the instability onset of the cubic lid-driven cavity, the latter part of the past decade has seen some significant advances in this field [70,42,41,52,51]. Giannetti et al. [32] found, by means of the first TriGlobal linear stability analysis applied to this kind of flows, that a stationary mode becomes unstable just above $Re \sim 2000$. The latter results is consistent with that of Liberzon et al. [53,30], who refined the prediction of Giannetti et al. [32] and experimentally and numerically found that the flow becomes oscillatory at $Re > 1970$ and a steady–unsteady transition occurs in the range $1700 < Re < 1970$. This kind of steady–unsteady transition has been also observed by Aidun, Benson et al. [1,12] and Chiang et al. [21,20] in a cavity of aspect ratio $1:1:3$, and by Albensoeder and Kuhlmann [3] with a very long cavity of aspect ratio $1:1:6.55$.

In order to alleviate disagreements in the numerical results of three-dimensional cavity flows [70,42,41,52,51], Albensoeder and Kuhlmann [2] created benchmark data of the three-dimensional cubic lid-driven cavity flow by employing high-order spectral collocation schemes. They show that rather high resolutions of $N^3 = 96$ spectral collotation nodes are required for an accurate description of the flow at $Re = 1000$. The lack of such resolution in several previous studies by other authors could explain most disagreements. Taking this benchmark data into account, Feldman and Gelfgat [30] made use of a resolution up to $N^3 = 200$ for their research of the cubic lid-driven cavity stability, while Liberzon et al. [53] validated the results of Feldman and Gelfgat [30] experimentally. At this point, considering the employed resolutions for an accurate description of the flow in previous works, it is to be expected that computational cost required for a TriGlobal instability analysis of the three-dimensional wall-bounded lid-driven cavity using second-order methods can become formidable and can be considered a challenge for the methodology presented in this paper.

The rest of this paper is organized as follows. First, in Section 2, linear stability theory in a time-stepping context is discussed. Next, in Section 3 the most important characteristics of the DNS codes used in the time-stepping are highlighted. Then, in Section 4 results are discussed, and conclusions are presented in Section 5.

2. Theory

2.1. TriGlobal linear stability analysis

The three-dimensional dimensionless Navier–Stokes equations of a viscous, incompressible fluid in Cartesian coordinates can be written as:

$$\nabla \cdot \mathbf{u} = 0, \tag{1}$$

$$\frac{\partial \mathbf{u}}{\partial t} + \mathbf{u} \cdot \nabla \mathbf{u} = -\nabla p + \frac{1}{Re} \nabla^2 \mathbf{u} \tag{2}$$

where Re is the Reynolds number, $\mathbf{u} = (u, v, w)$ is the velocity vector expressed in Cartesian coordinates (x, y, z) and p is the pressure. For the proposed validation problem, the three-dimensional lid-driven cavity, the Reynolds number Re is based on the lid speed and length in the x-direction and no-slip boundary conditions $u = v = w = 0$ are applied at all the boundaries, except in the lid-driven wall, where $u(x, y, z) = 1$.

The above-mentioned three-dimensional and dimensionless Navier–Stokes equations (2) can be written in compact form as:

$$\frac{\partial \mathbf{u}}{\partial t} = \mathbf{f}(\mathbf{u}), \tag{3}$$

where $\mathbf{u}$ contains the (divergence-free) three velocity components in the computational nodes.

The flow is decomposed in a base flow $\bar{\mathbf{u}}$ and three-dimensional amplitude function of the unsteady small perturbations $\epsilon \mathbf{u}'$ with $\epsilon \ll 1$,

$$\mathbf{u}(x, y, z, t) = \bar{\mathbf{u}}(x, y, z, t) + \epsilon \mathbf{u}'(x, y, z, t). \tag{4}$$

A linearized eigenvalue problem can be written taking this assumption into the Navier–Stokes equation (3), retaining the $O(\epsilon)$ infinitesimal terms:

$$\frac{\partial \mathbf{u}'}{\partial t} = \frac{\partial \mathbf{f}(\bar{\mathbf{u}})}{\partial \mathbf{u}} \mathbf{u}' \equiv \mathbf{A}\mathbf{u}', \tag{5}$$

where $\mathbf{A}$ is the Jacobian matrix of the right-hand side of the Navier–Stokes equation. According to the TriGlobal ansatz [75], solutions of Eq. (5) are sought as eigenmodes:

$$\mathbf{u}'(x, y, z, t) = \hat{\mathbf{u}}(x, y, z) e^{\lambda t} + \text{c.c.} \tag{6}$$

where $\lambda = \lambda_r + i \cdot \lambda_i$, with λ_i representing a frequency and λ_r being the amplification/damping rate of the disturbance sought and c.c. the complex conjugate and $\hat{\mathbf{u}}$ are the eigenfunctions. Coupling this modal solution (6) into the linearized equation (5) leads to the eigenvalue problem:

$$\lambda \hat{\mathbf{u}} = \mathbf{A}\hat{\mathbf{u}} \tag{7}$$

which will be numerically solved with the methodology described next.

3. Numerical method

3.1. Matrix-free framework

The present methodology is based on a matrix-free framework directly employing a non-linear DNS solver instead of using a linearized version. By following the Newton iteration [48], which is equivalent to applying a Taylor series expansion to the Navier–Stokes equation around the steady base flow $\bar{\mathbf{u}}$ and considering that the second and higher-order terms with respect to $\epsilon\mathbf{u}'$ are negligibly small, it can be written that

$$\mathbf{f}(\bar{\mathbf{u}}+\epsilon\mathbf{u}') = \mathbf{f}(\bar{\mathbf{u}}) + \frac{\partial \mathbf{f}(\bar{\mathbf{u}})}{\partial \mathbf{u}}\epsilon\mathbf{u}' + O(\epsilon^2), \tag{8}$$

and a Jacobian-vector product can be then obtained means of:

$$\frac{\partial \mathbf{f}(\bar{\mathbf{u}})}{\partial \mathbf{u}}\mathbf{u}' \approx \frac{\mathbf{f}(\bar{\mathbf{u}}+\epsilon\mathbf{u}') - \mathbf{f}(\bar{\mathbf{u}})}{\epsilon}. \tag{9}$$

This equation is also known as a Frèchet derivative [46] and it provides the Jacobian-vector product by the sum of two vectors corresponding to the right-hand side of the Navier–Stokes equations, which can be directly obtained from a non-linear DNS solver. High-order Frèchet derivatives can be created by increasing the stencil.

3.2. Jacobian-free Newton–Krylov methods

Jacobian-free Newton–Krylov [48] (JFNK) methods are Krylov subspace projection-iterative methods that make use of the Frèchet derivative or Newton iteration described in the previous subsection to solve generalized eigenproblems. The most popular JFNK methods follow the classic Arnoldi [67,7] algorithm, which consists of the generation of a Krylov subspace and its orthonormalization in order to create a reduced matrix that contains the leading eigenvalues of the original Jacobian matrix. An orthonormal base $\mathbf{U}$ of an m-dimensional Krylov subspace is generated with an initial vector and successive applications of the Jacobian matrix following a Gram–Schmidt orthonormalization step. Projecting the Jacobian matrix onto this orthonormal basis, its approximation:

$$\mathbf{AU} \sim \mathbf{UH}, \tag{10}$$

is obtained, where $\mathbf{H}$ is an $m \times m$ Hessenberg matrix obtained via a Gram–Schmidt orthonormalization procedure that contains an approximation of the eigenvalues of the Jacobian matrix $\mathbf{A}$. Performing an eigenvalue decomposition of the Hessenberg matrix $\mathbf{H} = \mathbf{D}\boldsymbol{\Lambda}\mathbf{D}^{-1}$, Eq. (10) can be written as:

$$\mathbf{A} \sim \mathbf{UD}\boldsymbol{\Lambda}\mathbf{D}^{-1}\mathbf{U}^{T}, \tag{11}$$

where the eigenvalues of the diagonal matrix $\boldsymbol{\Lambda}$ are approximations of the eigenvalues of the Jacobian matrix $\mathbf{A}$ and $\mathbf{UD}$ are approximations of the eigenfunctions or global modes. The major advantage of this algorithm is its matrix-free nature and its ability to make use of a non-linear DNS. The eigenvalue problem is solved by using Jacobian matrix perturbation vector products and these matrix-vector products are obtained by the sum of two vectors via the Frèchet derivative and a non-linear DNS as described in the previous subsection.

3.3. The present methodology

The present methodology is based on the Chiba approach [22,23], which links a Jacobian-free Newton–Krylov method [48] that follows the classic Arnoldi [7] algorithm, with a temporal exponential transformation of the spectrum. This spectrum transformation is required for the conversion of the leading eigenvalues (eigenvalues with largest real part) into the dominant eigenvalues (eigenvalues with largest modulus), which are the ones that the Arnoldi method can recover. Integrating the linearized equation (5) over a time τ and using the TriGlobal ansatz (6) leads to the exponential of the eigenvalue problem:

$$e^{\lambda\tau}\hat{\mathbf{u}} = \mathbf{e}^{\mathbf{A}\tau}\hat{\mathbf{u}}, \tag{12}$$

the spectrum of which corresponds to the exponential of the original Jacobian matrix. Fig. 2 represents the temporal exponential transformation of the spectrum. In this figure it can be seen how the leading eigenvalue of the Jacobian matrix (circle) becomes the dominant in the spectrum of the exponential of the Jacobian matrix. At the same time, the original dominant eigenvalues (square and diamond) are shifted to zero. Therefore, the eigenvalue solution can be obtained with following the Arnoldi method, with the particularity of substituting the Jacobian operator $\mathbf{A}$ with its exponential $e^{\mathbf{At}}$. Integrating a time τ the original Frèchet derivative (9) and recalling the linearized Navier–Stoke equation (5), the exponential of the Frèchet derivative can be written as:

$$e^{\mathbf{A}\tau}\mathbf{u}' \approx \frac{\int_0^{\tau}(\mathbf{f}(\bar{\mathbf{u}}+\epsilon\mathbf{u}') - \mathbf{f}(\bar{\mathbf{u}}))\,\mathrm{d}t}{\epsilon}, \tag{13}$$

which provides the exponential of the Jacobian-vector product by the sum of two vector obtained by the temporal integration of the non-linear DNS.

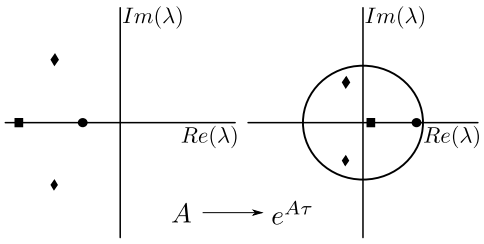

Fig. 2. Temporal exponential transformation.

The major algorithmic contribution of this paper to this methodology is to examine whether *any* non-linear DNS can be used in a *black-box* manner in order to provide the matrix-vector products required for the stability problem. From an algorithmic point view, this would mean that the stability and DNS problems can be treated separately and it would be possible to easily couple the present stability algorithm with in principle any DNS code, without modifying neither the stability analysis solver not the DNS in any aspect. The open source software OpenFOAM has been employed to perform the three-dimensional direct numerical simulations in this work. Although the high quality performance of this solver in an instability analysis context has been already demonstrated [17,16,68], an independent validation of this solver is carried out in the next section. Taking into account the utilization of OpenFOAM along with the previous descriptions of JFNK methods following the Arnoldi iteration and temporal exponential transformations, the full methodology is detailed in Algorithm 1.

Fig. 3 shows the flux diagram of the present algorithm steps coupled with an OpenFOAM, where only the I/O routines need to be modified if a different DNS solver were to be used.

3.4. Parameters selection

The most challenging aspects of the proposed methodology is the adequate selection of the input parameters shown in Fig. 3, namely the integration time τ, perturbation magnitude ϵ and the Krylov subspace dimension m, all of which must be selected by the user. This subsection provide some guidelines for their appropriate selection.

Algorithm 1 Present methodology.

S1. Initial condition: Set m, ϵ and $\mathbf{u}'_1$
S2. Arnoldi iteration: Perform until convergence ($l = 1, \ldots, m$),
  A1. Call OpenFOAM: $\mathbf{u}_{\mathbf{l}+} = \bar{\mathbf{u}}(\tau) + \epsilon \mathbf{u}'_l(\tau)$ and $\mathbf{u}_{\mathbf{l}-} = \bar{\mathbf{u}}(\tau) - \epsilon \mathbf{u}'_l(\tau)$
  A2. Compute Frèchet derivative through vector sum: $e^{\mathbf{A}\tau}\mathbf{u}'_l = \frac{\mathbf{u}_{\mathbf{j}+} - \mathbf{u}_{\mathbf{j}-}}{2\epsilon}$
  A3. Gram–Schmidt orthonormalization: ($i = 1, \ldots, l$)
    GS1. Form Hessenberg matrix $h_{il} = \mathbf{u}'^{T}_i e^{\mathbf{A}\tau}\mathbf{u}'_l$
    GS2. Orthogonalize $\mathbf{u}'_{l+1} = e^{\mathbf{A}\tau}\mathbf{u}'_l - \sum_{i=1}^{j} h_{il}\mathbf{u}'_i$
    GS3. Normalize $h_{l+1,l} = \|\mathbf{u}'_{l+1}\|$, $\mathbf{u}'_{l+1} = \frac{\mathbf{u}'_{l+1}}{h_{l+1,l}}$
S3. QR: Perform eigenvalue decomposition of the $m \times m$ matrix **H**
S4. Undo exponential transformation

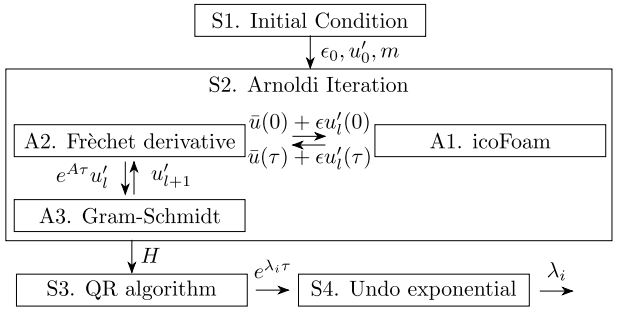

Fig. 3. Flux diagram of the proposed algorithm (left) instability routines (middle) auxiliary routines (right) DNS routines.

Criteria for the selection of the integration time τ can be found in the early work of Goldhirsch et al. [33], where it is stated that one of the necessary conditions for the recovery of the eigenvalue λ_i using iterative projection methods is

$$|\lambda_i - \lambda_m|\tau \gg 1. \tag{14}$$

This condition ensures that the sought eigenvalues are sufficiently separated from the rest in the exponential transformation of the spectrum, so that they can be recovered with the Arnoldi algorithm, as it was shown in Fig. 2. Satisfaction of this condition can be achieved either by increasing the dimension m of the Krylov subspace or by increasing the length of the temporal integration τ. Both options are equivalent in terms of computational effort, however increasing τ has turned out as the best option in this work, since the leading eigenvalues of the studied spectra studied in the present work are close to each other. Another essential aspect is the control of the perturbation magnitude, since the equations that are being integrated are not linear and the perturbation must remain linear. While Knoll and Keyes [48] review advanced techniques in order to control the perturbation magnitude, the original criterion envisaged by Eriksson and Rizzi [28] has proven to be effective in the present context. One ensures that the perturbation magnitude is related with the L2 norm of the base flow and perturbation vectors through:

$$\epsilon = \epsilon_0 \frac{\|\bar{\mathbf{u}}\|}{\|\mathbf{u}'\|}, \tag{15}$$

where the constant ϵ_0 represents the initial order of magnitude of the residual of the temporal integration. A value of $\epsilon_0 \sim 10^{-5}$ has been used throughout this work. In addition, attention must be paid to the truncation error of the Frèchet derivative, since the order of magnitude of this error ($O(\epsilon^2)$) can be bigger than the absolute residual tolerance of the numerical scheme ϵ_m, which denotes the accuracy or number of correct significant figures of the solution provided by the DNS.

This issue can be resolved by computing the Frèchet derivative using a second or higher order. Finally, the initial order of magnitude of the perturbation ϵ_0 and the length of the temporal integration τ can be related with the condition that the residual of the integration remains bigger than the residual tolerance of the numerical scheme ϵ_m, namely

$$\epsilon_0 e^{\lambda_1 \tau} > \epsilon_m. \tag{16}$$

Finally, an upper and lower limit to the length of integration τ can be established taking into account the previous expression and Eq. (14) as

$$\frac{1}{\lambda_i - \lambda_m} < \tau < \frac{\ln(\frac{\epsilon_m}{\epsilon_0})}{\lambda_1}. \tag{17}$$

Experience gained in the present work suggested that this expression may be used to indicate that when left- and right-hand side of the equation have the same order of magnitude, the Krylov subspace dimension needs to be increased.

4. Results

4.1. Base flow

The base flow results of the cubic lid-driven cavity at $Re = 1000$ have served as validation case of the capability to run an incompressible solver of OpenFOAM in DNS mode; a grid convergence analysis has been carried out, then the obtained steady-state solution has been compared with the benchmark data created by Albensoeder et al. [2] and the transient solver quality have tested comparing the damping ratio using the residual algorithm described in Theofilis [76].

The transient incompressible solver icoFoam has been employed to obtain the base flow. This solver discretizes the incompressible Navier–Stokes equations using the classic finite volume formulation and a PISO [44,31] (Pressure Implicit with Splitting of Operators) velocity-pressure coupling method with a second-order Crank–Nicholson method as temporal scheme. In addition, a GAMG (Geometric Agglomerated Algebraic Multigrid) linear solver has been used for the solution of pressure equation. The base flow is calculated by advancing in time the Navier–Stokes equations from a quiescent initial condition until the residual satisfies a predetermined convergence criterion. This residual $\varepsilon(t)$ is defined at each time t as the $L1$ norm of the discretized residual vector

$$\mathbf{u}_r(t) = \frac{\partial \mathbf{u}(t)}{\partial t} + \mathbf{u}(t) \cdot \nabla \mathbf{u}(t) - \frac{1}{Re}\nabla^2 \mathbf{u}(t) + \nabla p(t), \tag{18}$$

normalized by the initial residual $\varepsilon(0)$. A residual tolerance for the temporal integration $\varepsilon(t) < \epsilon_m$ with $\epsilon_m = 10^{-12}$ has been found sufficient for this work.

A grid refinement study based on a generalized Richardson extrapolation method [65], as used by Sanmiguel-Rojas et al. [68] has been employed in order to analyze mesh convergence. The method consists of constructing a grid convergence index [65] (GCI) that acts as a measure of the behavior of the numerical solution as it approaches a grid-independent asymptotic value, following the Richardson extrapolation method. This grid convergence index [65] can be defined as:

$$GCI_{j+1,j} = 3 \times \left| \frac{u_{j+1} - u_j}{u_j(l^n - 1)} \right| \times 100, \tag{19}$$

where u_j is any variable discretized on mesh j, where mesh $j+1$ is coarser than mesh j, l is the fine-to-coarse grid size refinement ratio in one spatial direction and n is the order of convergence rate of the method. In addition, attention has to be paid in order to ensure that monotonic convergence has been achieved before applying the method. Furthermore, the grid-independent solution based on Richardson extrapolation can be estimated as

$$u_{re} \sim u_j + \frac{u_{j+1} - u_j}{(l^n - 1)}, \tag{20}$$

Table 1
Grid convergence study based on u velocity for the cubic lid-driven cavity at $Re = 1000$ using five meshes: from M1 (finest) to M5 (coarsest). Grid convergence index obtained with $l = 1.5$ and $n = 1.71$.

Mesh	N_x	N_y	N_z	N^3	$u(0.5, 0, 75, 0, 5)$	$GCI_{j+1,j}$ (%)	ϵ_j (%)
Grid-independent	–	–	–	–	0.07861	–	–
M1	216	216	216	$\sim 1 \times 10^7$	0.07859	0.54	0.02
M2	144	144	144	$\sim 3 \times 10^6$	0.07852	1.09	0.11
M3	96	96	96	$\sim 9 \times 10^5$	0.07837	2.01	0.29
M4	64	64	64	$\sim 2.5 \times 10^5$	0.07811	3.92	0.63
M5	42	42	42	$\sim 7.5 \times 10^4$	0.07759	–	1.29

Table 2
Comparison with the benchmark [2] spectral collocation method (SCM) solution of the minimum and maximum velocities on the centerlines $v(x, 0.5, 0.5)$ and $u(0.5, y, 0.5)$ for the cubic lid-driven cavity at $Re = 1000$.

Method	AR	N_x	N_y	N_z	v_{min}	x	v_{max}	x	u_{max}	y
SCM	1 : 1 : 1	96	96	64	−0.4350	0.9096	0.2466	0.1091	−0.2803	0.1242
FVM	1 : 1 : 1	144	144	144	−0.4333	0.9076	0.2456	0.1073	−0.2792	0.1235
FVM	1 : 1 : 1	96	96	96	−0.4332	0.9101	0.2444	0.1117	−0.2777	0.1284
FVM	1 : 1 : 1	64	64	64	−0.4280	0.9079	0.2416	0.1148	−0.2746	0.1274
SCM	1 : 1 : 2	96	96	96	−0.4736	0.9108	0.2941	0.1305	−0.3197	0.1306
FVM	1 : 1 : 2	64	64	128	−0.4604	0.9079	0.2852	0.1151	−0.3127	0.1408
SCM	1 : 1 : 3	96	96	96	−0.4901	0.9097	0.3235	0.1237	−0.3444	0.1367
FVM	1 : 1 : 3	64	64	192	−0.4687	0.9079	0.3001	0.1274	−0.3219	0.1549

so the corresponding relative percentage error of each mesh compared to the grid-independent solution is defined as:

$$\epsilon_j = \left| \frac{u_j - u_{re}}{u_{re}} \right| \times 100. \tag{21}$$

Table 1 presents the convergence results obtained with the incompressible OpenFOAM solver for five meshes with different resolutions of the cubic lid-driven cavity flow at $Re = 1000$. A cubic mesh with a linear stretching function of 1 : 8 ratio has been employed in order to solve accurately the flow in the vicinity of the lid and cavity walls and corners. The velocity in the direction of the lid movement u in the point $(0.5, 0.75, 0.5)$ has been selected as probe in order to alleviate the influence of the mesh stretching in the three directions towards the walls on the GCI.

Results shown in Table 1 demonstrate the slow improvement in accuracy as resolution is increased, due to the second-order accuracy of the numerical discretization even with a fine-to-coarse grid size refinement ratio $l = 1.5$ in each direction. It can be seen that the GCI-based on the velocity component u in the lid direction indicates than the mesh M2 with $\sim 3 \times 10^6$ cells is necessary to accurately predict the flow in the lid-driven cavity at $Re = 1000$, although the relative error criterion suggests that the resolution employed in mesh M4 may be sufficient to describe the flow this Reynolds number value. Fig. 4 shows comparisons of normal velocities at the centerlines $(x, 0, 0)$ and $(0, y, 0)$ of the cubic lid-driven cavity at $Re = 1000$, calculated on meshes M3 and M4, against the reference value. Table 2 quantifies the values of absolute maximum and minimum velocity at three different spanwise aspect ratios and shows that the maximum discrepancies from the reference solution are of order $O(10^{-3})$. These minimal differences in base flows obtained on the grids M2, M3 and M4 suggest that any of these grids may provide quantitatively comparable stability analysis results.

In addition, a study of different large aspect ratio cavities flow has been carried out on meshes with same resolution as M2 and M3. Results are also shown in Table 2, where a discrepancy of $O(10^{-2})$ from the reference solution can be seen. The accuracy of these base flows is also sufficient for the purposes of the present analyses, as will be shown in the next section.

Finally, the transient behavior of the solver has been also validated by means of the residual algorithm developed by Theofilis

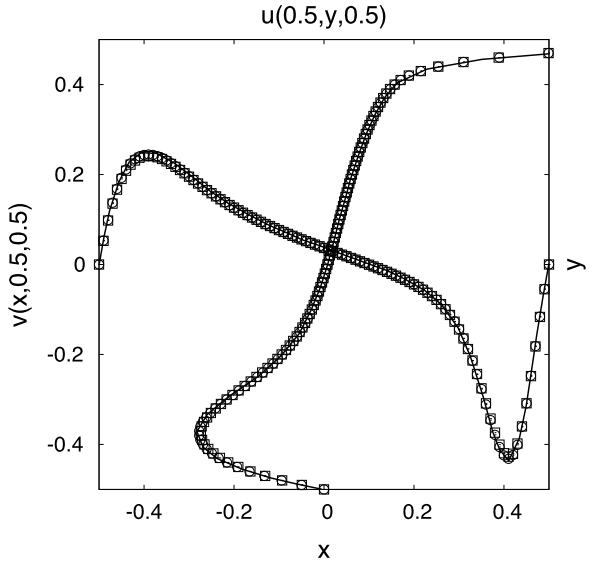

Fig. 4. Comparisons of normal velocities in the central lines $(x, 0, 0)$ y $(0, y, 0)$ of cubic lid-driven cavity at $Re = 1000$. Lines corresponds to reference values [2], and circle and squares to mesh M4 $N^3 = 64^3$ and mesh M3 $N^3 = 96^3$ respectively.

[74,76,34]. The key idea of this algorithm is that when time-accurate integration of the equations of motion is started from a random initial condition, if the solution approaches a steady state, the path to the latter is conditioned by the damping of the least stable flow eigenmodes. As such, during the time prior to convergence the residual is governed by only the leading damped linear global mode. In the particular case of a steady leading mode, recalling the definition of residual from Eq. (18), the corresponding damping ratio can be extracted from the logarithmic derivative of the signal, which reads

$$\lambda_1 = \frac{\ln(\frac{\epsilon(t+\Delta t)}{\epsilon(t)})}{\Delta t}. \tag{22}$$

Fig. 5 shows the temporal evolution of the residual of the two-dimensional lid-driven cavity at $Re = 1000$, in which the constant slope of the residual decay corresponds to the damping

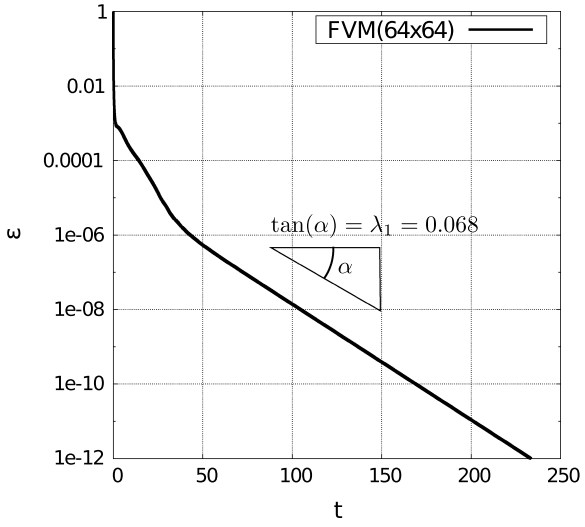

Fig. 5. Temporal evolution of the velocity residual of the two-dimensional singular lid-driven cavity at $Re = 1000$.

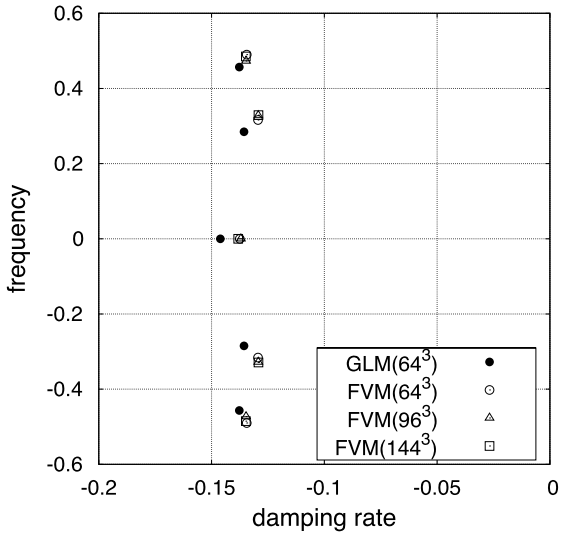

Fig. 6. Spectrum of cubic lid-driven cavity at $Re = 1000$ calculated by Giannetti et al. [32] (GLM) and own methodology (FVM) with different resolutions.

ratio and thus can be recovered with the previous expression. For this particular case, the recovered damping ratio corresponds to $\lambda_1 = 0.068$, which perfectly matches the value available in the literature [78] of $\lambda_{ref} = 0.068$. The same procedure will be used to cross-verify damping rate results of the time-stepping algorithm in the cubic lid-driven cavity against those delivered by this basic signal processing technique.

4.2. TriGlobal instability analyses

Validation of the present three-dimensional global (TriGlobal) instability analysis algorithm has been provided by comparison against reference works, starting with those of Giannetti et al. [32] at $Re = 1000$. Krylov subspace dimensions ranging from $m = 12$ to $m = 48$ have been tested along with integration times from $\tau = 10$ to $\tau = 100$ for the instability analysis. It has been found sufficient to use a Krylov subspace dimension $m = 12$ with integration time $\tau = 40$ for the recovery of the three first leading eigenvalues, satisfying the criteria discussed in the previous section. The recovered eigenvalues calculated with three different meshes M2, M3 and M4 can be seen in Table 3. Comparison between the reference spectrum of Giannetti et al. [32] and the present results obtained with these three different meshes can be seen in Fig. 6. An overall good agreement between the location of the eigenvalues can be seen, while the differences can be explained by the different numerical methods employed. Fig. 7 shows the eigenfunctions corresponding to these three least stable eigenvalues. The first two are traveling, corresponding to $\lambda_1 = -0.1292 \pm i \cdot 0.329$, $\lambda_2 = -0.138 \pm i \cdot 0.457$, while the third is a stationary eigenmode with a damping ratio $\lambda_3 = -0.146$. At this Reynolds number, it is observed that the two first eigenvalues are related to the corresponding modes of the two-dimensional flow, properly affected by the presence of the wall and thus the above-mentioned EWV structure. However, the existence of different n-cell symmetric and asymmetric families of linear modes with TGL structure may be inferred from the third mode.

Stability analysis at $Re = 2000$ close to the instability onset has also been performed on the coarser meshes M3 and M4. Fig. 8 shows the temporal evolution of the flow using these two meshes. The flow is shown to be stable using the coarsest resolution of $N^3 = 64$, a fact which can be attributed to the insufficient resolution to capture the salient flow features. Fig. 8 also shows that the residual decays with a damping ratio of $O(10^{-2})$ and that the mode is traveling. A stability analysis of the obtained steady base flow provides a traveling mode with an eigenvalue $\lambda_1 = 0.0095 \pm i \cdot 0.091$ and the corresponding eigenfunction with TGL shape is shown in Fig. 10. It needs to be noticed that the discrepancy in the obtained instability results using the mesh M3 has the same order of magnitude than the damping ratio and thus only affects this, while the obtained frequency, with a bigger order of magnitude, is not affected by this discrepancy and is in good agreement with the results found by Liberzon, Feldman and Gelfgat [53,30]. In addition, results in Fig. 8 show that the flow is non-linear at $Re = 2000$ using a resolution of $N^3 = 96$ and three different oscillatory regimes can be identified: (a) an unstable oscillatory flow, the frequency of which matches that of the leading eigenmode, (b) the corresponding linear saturation of this mode and (c) a quasi-steady oscillatory regime with a smaller frequency. The temporal evolution of the residual of these three regimes is shown in detail in Fig. 9. This behavior of the flow has been described as competition between modes with different pairs of TGL vortices by Aidun et al. [1], Guermond et al. [40] or as steady–oscillatory transition by Liberzon, Feldman and Gelfgat [53,30], with the presence of a steady-mode. Although the accurate physical interpretation of these numerical results lies beyond the objective of this paper, these phenomena could be explained with the existence of a limit cycle, as Fig. 8 shows.

The steady-state solver of OpenFOAM based on the SIMPLE method [31] has been employed to calculate an unstable steady base flow at $Re = 2000$ and resolution $N^3 = 96$, however the difference between the obtained results with the transient solver and the steady-state solver has an order of magnitude of $O(10^{-4})$,

Table 3
Effect of resolution on the first three leading eigenvalues of the lid-driven cavity at $Re = 1000$.

$N_x \times N_y \times N_z$	λ_1	λ_2	λ_3
$144 \times 144 \times 144$	$-0.1292 \pm i \cdot 0.329$	$-0.1348 \pm i \cdot 0.485$	$-0.1382 \pm i \cdot 0.000$
$96 \times 96 \times 96$	$-0.1293 \pm i \cdot 0.328$	$-0.1347 \pm i \cdot 0.473$	$-0.1370 \pm i \cdot 0.000$
$64 \times 64 \times 64$	$-0.1294 \pm i \cdot 0.316$	$-0.1344 \pm i \cdot 0.490$	$-0.1375 \pm i \cdot 0.000$

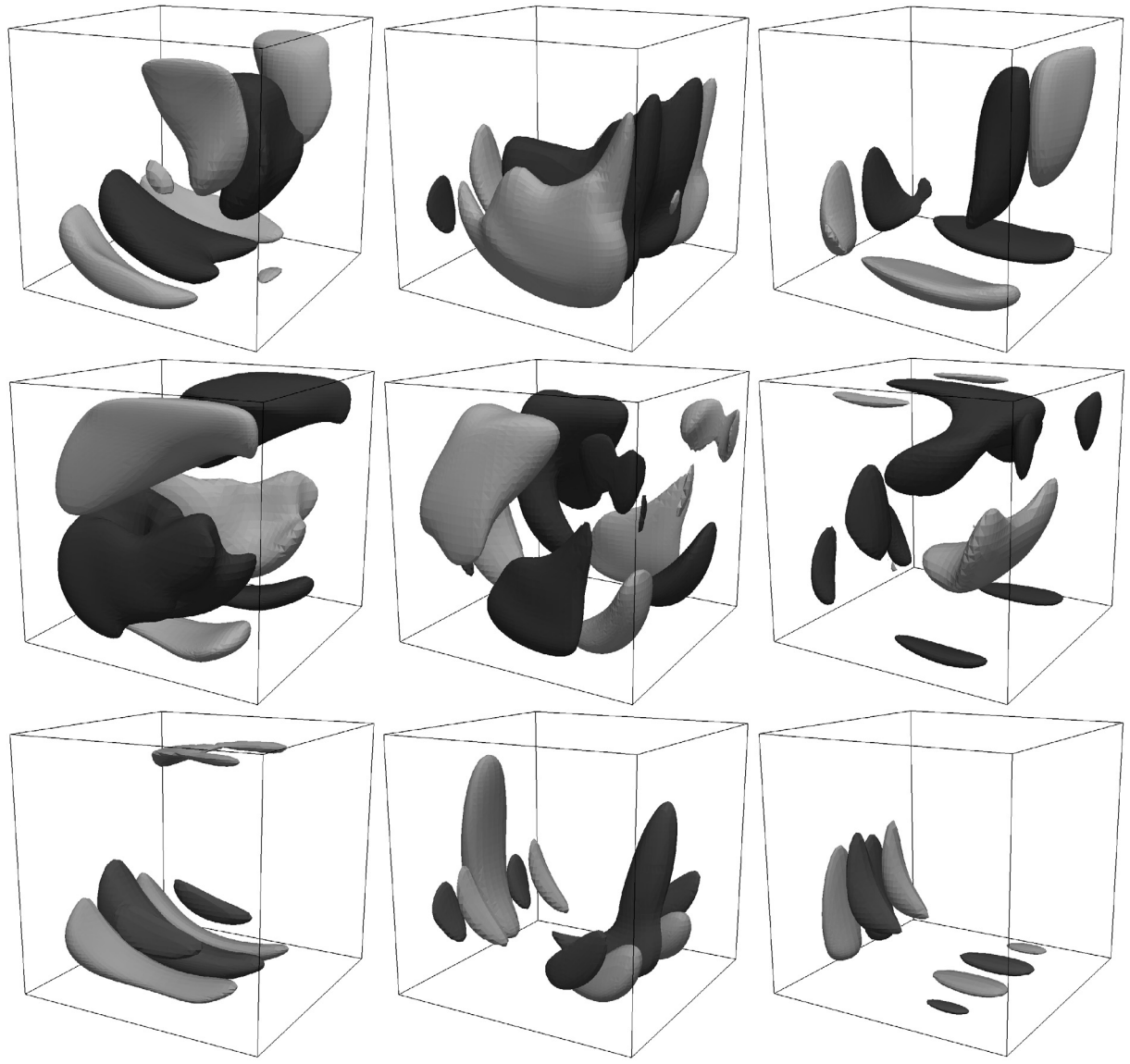

Fig. 7. Real part of the eigenfunction velocity field $(\hat{u}, \hat{v}, \hat{w})$ of the cubic lid-driven cavity at $Re = 1000$. Eigenfunctions normalized with $\max(\hat{u})$, lid moves from left to right. Resolution $N^3 = 96$. (*Top*): $\lambda_1 = -0.136 \pm i \cdot 0.285$ showing $\hat{u}, \hat{v}, \hat{w} = \pm 0.3$, (*middle*): $\lambda_2 = -0.138 \pm i \cdot 0.457$ showing $\hat{u}, \hat{v}, \hat{w} = \pm 0.3$, (*bottom*): $\lambda_3 = -0.146$ showing $\hat{u}, \hat{v}, \hat{w} = \pm 0.15$.

and this difference is bigger than the magnitude of the small initial linear perturbation that needs to be superimposed (typically $O(10^{-5})$, see Eq. (15)) upon the base flow computed with the transient solver. Thus the temporal evolution of the linear perturbation cannot be correctly computed with the transient solver because the presence of a bigger numerical error. As a result the base flow obtained with the steady-state solver of OpenFOAM cannot be analyzed with the present instability methodology.

Next, the flow features of lid-driven cavities with aspect ratio different to unity have been explored for the first time in a global instability analysis context using the proposed methodology. Regarding the spatial structure of the eigenfunctions of large aspect ratio cavities, the existing pattern of different n-cell symmetric and asymmetric families of modes can be found in all aspect ratios studied. As an example, the two least-stable eigenfunctions of the lid-driven cavity of aspect ratio $AR = 1:1:2$ and $AR = 1:1:3$ at $Re = 1000$ are shown in Figs. 11 and 12, where symmetric and asymmetric n-cell patterns of TGL vortices can be observed. The corresponding damping ratios of the leading eigenvectors at this Reynolds number are $\lambda_1 \sim 0.05$ for the $AR = 1:1:2$ cavity and

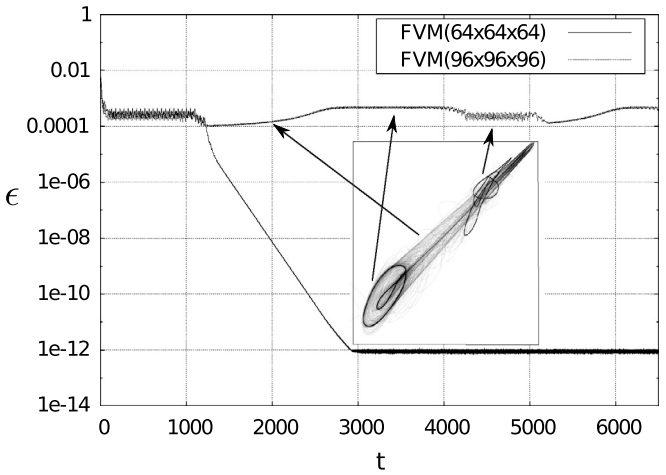

Fig. 8. Temporal evolution of the velocity residual of the cubic three-dimensional singular lid-driven cavity at $Re = 2000$.

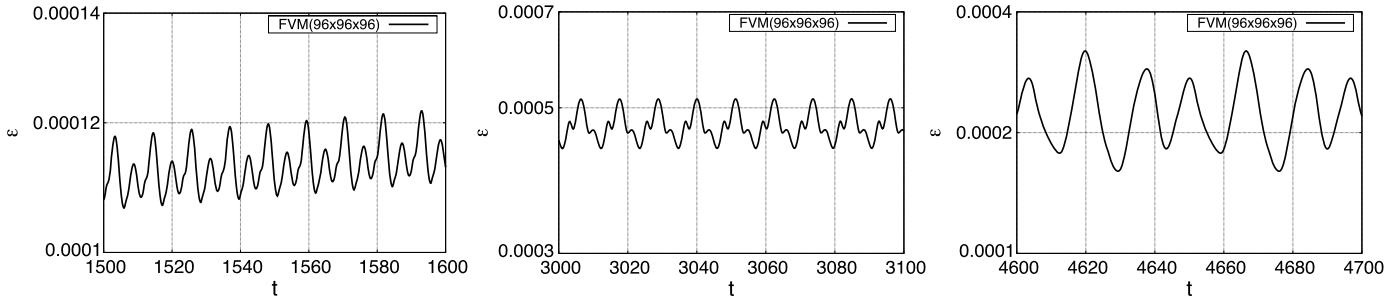

Fig. 9. Three different states in the temporal evolution of the velocity residual of the cubic three-dimensional singular lid-driven cavity at $Re = 2000$ zoomed from Fig. 8.

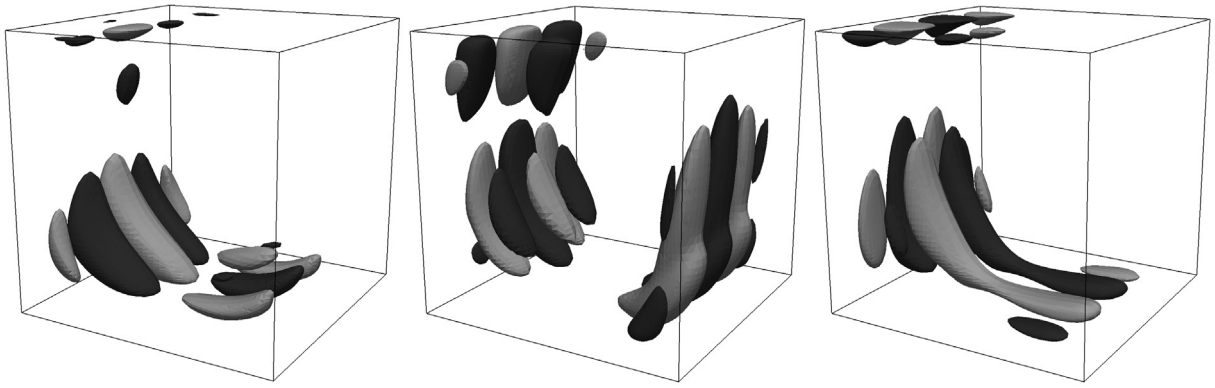

Fig. 10. Real part of the eigenfunction velocity field $(\hat{u}, \hat{v}, \hat{w})$ of the cubic lid-driven cavity at $Re = 2000$. Eigenfunction normalized with $\max(\hat{u})$. Showing $\hat{u}, \hat{v}, \hat{w} = \pm 0.1$, lid moves from left to right. $N^3 = 64$. $\lambda_1 = -0.095 \pm i \cdot 0.091$.

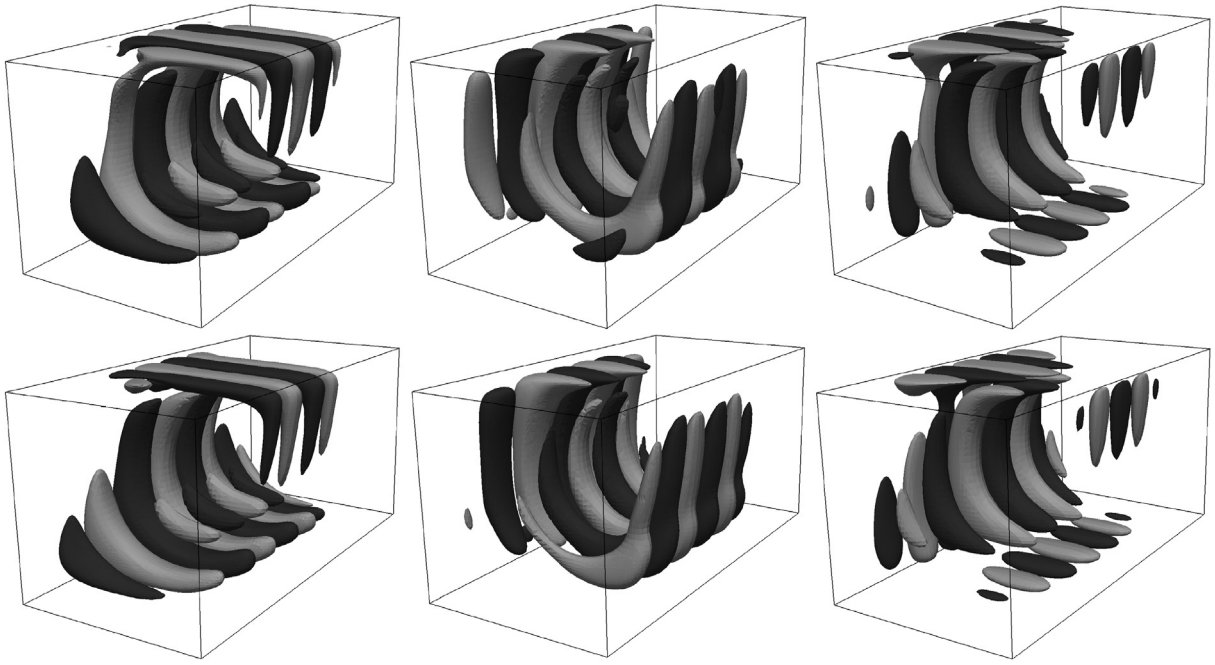

Fig. 11. Real part of the eigenfunction velocity field $(\hat{u}, \hat{v}, \hat{w})$ of the leading (*top*) and second (*bottom*) eigenmodes of the $AR = 1:1:2$ lid-driven cavity at $Re = 1000$. Eigenfunctions normalized with $\max(\hat{u})$. Showing $\hat{u}, \hat{v}, \hat{w} = \pm 0.1$, lid moves from left to right.

$\lambda_1 \sim 0.03$ $AR = 1:1:3$ cavity. These modes are in agreement with the damped TGL flow structures found in the start-up experiments and simulation carried out by Aidun et al. [1], Guermond et al. [40] and Migeon [55].

Moreover, Table 4 contains the three least-stable eigenvalues of different aspect ratio lid-driven cavities at a low Reynolds number $Re = 200$, where the strong influence of the wall on the flow stability may be appreciated. It is remarkable that the cavity of $AR = 1 : \frac{1}{3} : \frac{1}{3}$ is one order of magnitude more stable than the cubic lid-driven cavity, which is agreement with the findings of Albensoeder and Kuhlmann [3], who showed that TGL vortices are not formed close to the wall-end in large aspect ratio cavities. Next, independent increases of the aspect ratio parameters A_z or A_y have been performed in order to document their effect on flow stability; it was found that an increase in aspect ratio decreases the stability of the flow in both directions, as can also be seen in Table 4.

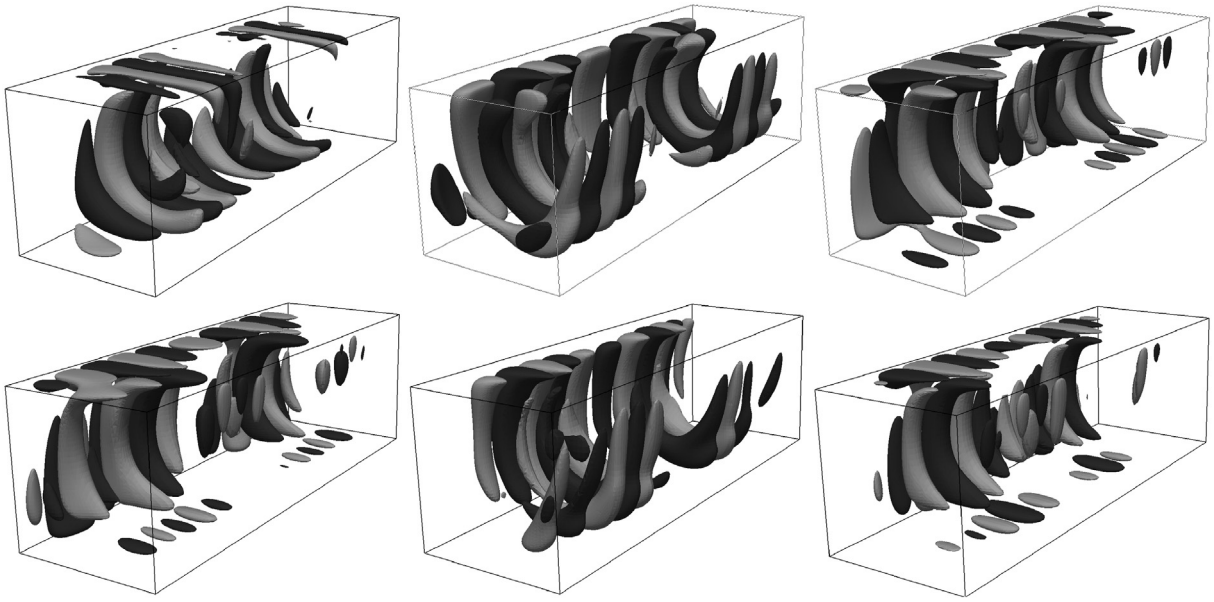

Fig. 12. Real part of the eigenfunction velocity field $(\hat{u}, \hat{v}, \hat{w})$ of the leading (*top*) and second (*bottom*) eigenmodes of the $AR = 1:1:3$ lid-driven cavity at $Re = 1000$. Eigenfunctions normalized with $\max(\hat{u})$. Showing $\hat{u}, \hat{v}, \hat{w} = \pm 0.1$, lid moves from left to right.

Table 4
Effect of aspect ratio $AR = 1 : A_y : A_z$ on the first three leading eigenvalues of the lid-driven cavity at $Re = 200$.

$AR = 1 : A_y : A_z$	λ_1	λ_2	λ_3
$1:1:\infty$	$-0.332 \pm i \cdot 0.000$	$-0.551 \pm i \cdot 0.000$	$-0.981 \pm i \cdot 0.034$
$1:\frac{1}{3}:\frac{1}{3}$	$-2.111 \pm i \cdot 0.449$	$-2.285 \pm i \cdot 0.289$	$-2.710 \pm i \cdot 0.690$
$1:1:1$	$-0.403 \pm i \cdot 0.132$	$-0.435 \pm i \cdot 0.000$	$-0.547 \pm i \cdot 0.188$
$1:1:2$	$-0.310 \pm i \cdot 0.000$	$-0.337 \pm i \cdot 0.146$	$-0.369 \pm i \cdot 0.276$
$1:1:3$	$-0.278 \pm i \cdot 0.000$	$-0.332 \pm i \cdot 0.120$	$-0.352 \pm i \cdot 0.000$
$1:2:1$	$-0.240 \pm i \cdot 0.000$	$-0.322 \pm i \cdot 0.000$	$-0.324 \pm i \cdot 0.058$
$1:3:1$	$-0.235 \pm i \cdot 0.000$	$-0.239 \pm i \cdot 0.000$	$-0.256 \pm i \cdot 0.000$

Table 5
Computational costs of the instability analysis of the cubic LDC at $Re = 1000$ with $m = 12$ and $\tau = 40$ using different resolutions in a 8-processor workstation.

Mesh	N^3	Δt	T_{step} (s)	T_{total} (h)	Memory (GB)
M1	216^3	0.006	299.0	$O(10^5)$	30.1
M2	144^3	0.025	21.8	∼232	9.9
M3	96^3	0.05	14.1	∼75	3.6
M4	64^3	0.1	2.7	∼7.2	1.2

As a mere exercise, the residual of very long cavities of aspect ratio up to $AR = 1:1:40$ has been also investigated, finding a damping ratio very close to that obtained by BiGlobal linear analysis of spanwise homogeneous flows [78], $\lambda_1 = 0.3297$.

Finally a study of the computational cost for the analysis using the proposed algorithm is shown in Table 5. Information is provided on the required CPU time T_{total} and RAM memory for a stability analysis of the cubic LDC with each of the employed meshes using a Krylov subspace dimension $m = 12$ with an integration time $\tau = 40$. In addition, the required CPU time T_{total} for a complete instability analysis can be estimated as:

$$T_{total} \sim \frac{2m\tau T_{step}}{\Delta t}, \tag{23}$$

T_{step} being the employed CPU time by the solver for one numerical time step.

All simulations have been run in parallel on a 8-core workstation with 32 GB RAM memory. It is remarkable that the CPU time has been reduced by an order of magnitude because of the good properties of the employed mesh; due to the orthogonality of the mesh and its $1:8$ stretching towards the walls, it has been able to set maximum *CFL* numbers $CFL \sim 10$, avoiding numerical oscillations. This has been tested performing analysis using mesh M4 with $CFL < 0.3$ and $CFL \sim 10$, providing identical results. Moreover, it is also shown that calculation with resolutions beyond $N^3 = 144$ are not feasible in reasonable CPU times and even can lead to lack of RAM memory issues. These findings represent the limits of the proposed methodology, if reasonable computing times are to be employed for the instability analysis of three-dimensional laminar flows.

5. Conclusions

The development of a general approach for the solution of the TriGlobal linear instability analysis eigenvalue problem is presented, by coupling the open-source toolbox OpenFOAM with a matrix-free time-stepping methodology, including the algorithmic innovations necessary in order to perform such analysis. The ability to directly use software utilities available within the OpenFOAM open source package, such as parallelization, pre- or post-processing has been exploited. Guidelines have been provided for the adequate selection of the parameters of the proposed algorithm.

The methodology has been successfully validated against the available results in the literature for cubic lid-driven cavities at $Re = 1000$ and it has been further demonstrated to be capable of providing for the first time eigenvalues and eigenfunctions of the flow inside three-dimensional, wall-bounded lid-driven cavity flows of aspect ratio different to unity. Results were found in qualitative agreement with those available in the literature in a DNS

or experimental context. Moreover, it has been shown that linear eigenmodes presenting symmetric and asymmetric n-cell TGL patterns exist in stable flows, linking these well-known structures with linear global flow eigenmodes.

It can be concluded that the proposed algorithm enables TriGlobal linear modal instability analysis of flows in complex geometries on modest contemporary hardware and is a viable alternative to existing methods for the instability analysis of laminar flows in three-dimensional geometries, leaving the analysis of turbulent flows in such geometries as a future challenge.

Acknowledgements

Support of the Marie Curie Grant PIRSES-GA-2009-247651 *"FP7-PEOPLE-IRSES: ICOMASEF – Instability and Control of Massively Separated Flows"* is gratefully acknowledged.

References

[1] C.K. Aidun, N.G. Triantafillopoulos, J.D. Benson, Global stability of a lid-driven cavity with throughflow: Flow visualization studies, Physics of Fluids 3 (1991).
[2] S. Albensoeder, H. Kuhlmann, Accurate three-dimensional lid-driven cavity flow, Journal of Computational Physics 206 (2005) 536–558.
[3] S. Albensoeder, H.C. Kuhlmann, Nonlinear three-dimensional flow in the lid-driven square cavity, Journal of Fluid Mechanics 569 (2006) 465–480.
[4] S. Albensoeder, H.C. Kuhlmann, H.J. Rath, Three-dimensional centrifugal-flow instabilities in the lid-driven-cavity problem, Physics of Fluids 13 (2001) 121–136.
[5] S. Albensoeder, H.C. Kuhlmann, H.J. Rath, Multiplicity of steady two-dimensional flows in two-sided lid-driven cavities, Theoretical and Computational Fluid Dynamics 14 (2001) 223–241.
[6] S. Albensoeder, H.C. Kuhlmann, H.J. Rath, Three-dimensional centrifugal-flow instabilities in the lid-driven-cavity problem, Physics of Fluids 13 (2001) 121–136.
[7] W. Arnoldi, The principle of minimized iterations in the solution of the matrix eigenvalue problem, Quarterly of Applied Mathematics 9 (1951) 17–29.
[8] S. Bagheri, E. Åkervik, L. Brandt, D.S. Henningson, Matrix-free methods for the stability and control of boundary-layer flows, AIAA Journal 47 (2009) 1057–1068.
[9] S. Bagheri, P. Schlatter, P.J. Schmid, D.S. Henningson, Global stability of a jet in crossflow, Journal of Fluid Mechanics 624 (2009) 33–44.
[10] D. Barkley, R.D. Henderson, Three-dimensional Floquet stability analysis of the wake of a circular cylinder, Journal of Fluid Mechanics 322 (1996) 215.
[11] D. Barkley, H.M. Blackburn, S.J. Sherwin, Direct optimal growth analysis for timesteppers, International Journal for Numerical Methods in Fluids 57 (2008) 1435–1458.
[12] J.D. Benson, C.K. Aidun, Transition to unsteady nonperiodic state in a through-flow liddriven cavity, Physics of Fluids 4 (1992) 2316–2319.
[13] D. Biau, H. Soueid, A. Bottaro, Transition to turbulence in duct flow, Journal of Fluid Mechanics 596 (2008) 133–142.
[14] H. Blackburn, Three-dimensional instability and state selection in an oscillatory axisymmetric swirling flow, Physics of Fluids 14 (2002) 3983–3996.
[15] H.M. Blackburn, S. Sherwin, Formulation of a Galerkin spectral element-Fourier method for three-dimensional incompressible flows in cylindrical geometries, Journal of Computational Physics 197 (2004) 759–778.
[16] P. Bohorquez, L. Parras, Three-dimensional numerical simulation of the wake flow of an afterbody at subsonic speeds, Theoretical and Computational Fluid Dynamics 26 (2012) 201–218.
[17] P. Bohorquez, E. Sanmiguel-Rojas, A. Sevilla, J. Jimenez-Gonzalez, C. Martinez-Bazan, Stability and dynamics of the laminar wake past a slender blunt-based axisymmetric body, Journal of Fluid Mechanics 676 (2011) 110–144.
[18] V. Boppana, J. Gajjar, Global flow instability in a lid-driven cavity, International Journal for Numerical Methods in Fluids 62 (2010) 827–853.
[19] G.A. Bres, T. Colonius, Three-dimensional instabilities in compressible flow over open cavities, Journal of Fluid Mechanics 599 (2008) 309–339.
[20] T. Chiang, R. Hwang, W. Sheu, On end-wall corner vortices in a lid-driven cavity, Journal of Fluids Engineering 1119 (1997) 201–204.
[21] T. Chiang, W. Sheu, R. Hwang, Effect of Reynolds number on the eddy structure in a lid-driven cavity, International Journal for Numerical Methods in Fluids 26 (1998) 557–579.
[22] S. Chiba, Global stability analysis of incompressible viscous flow, Journal of Japanese Society of Computational Fluid Dynamics 7 (1998) 20–48.
[23] S. Chiba, Three-dimensional global stability analysis for the time-periodic cylinder wake, Theoretical Applied Mechanics (Japan) 50 (2001) 321–326.
[24] J. De Vicente, D. Rodriguez, V. Theofilis, E. Valero, Stability analysis in spanwise-periodic double-sided lid-driven cavity flows with complex cross-sectional profiles, Computers & Fluids 43 (2011) 143–153.
[25] H.A. Dijkstra, M.J. Molemaker, A. van der Ploeg, E.F.F. Botta, An efficient code to compute non-parallel flow steady flows and their linear stability, Computers & Fluids 24 (1995) 415–434.
[26] Y. Ding, M. Kawahara, Linear stability of incompressible fluid flow in a cavity using finite element method, International Journal for Numerical Methods in Fluids 27 (1998) 139–157.
[27] W. Edwards, L. Tuckerman, R. Friesner, D. Sorensen, Krylov methods for the incompressible Navier–Stokes equations, Journal of Computational Physics 110 (1994) 82–102.
[28] L. Eriksson, A. Rizzi, Computer-aided analysis of the convergence to steady state of discrete approximations to the Euler equations, Journal of Computational Physics 57 (1985) 90–128.
[29] E. Ertuck, Discussions on driven cavity flow, International Journal for Numerical Methods in Fluids 60 (2009) 275–294.
[30] Y. Feldman, A.Y. Gelfgat, Oscillatory instability of a three-dimensional lid-driven flow in a cube, Physics of Fluids 22 (2010) 093602 (10 pages).
[31] J. Ferziger, M. Peric, Computational Methods for Fluid Dynamics, Springer, 2001.
[32] F. Giannetti, P. Luchini, L. Marino, Linear stability analysis of three-dimensional lid-driven cavity flow, in: Atti del XIX Congresso AIMETA di Meccanica Teorica e Applicata, Ancona, 14–17 Sep., Aras Edizioni, Ancona, Italy, 2009, pp. 738.1–738.10.
[33] I. Goldhirsch, S.A. Orszag, B.K. Maulik, An efficient method for computing leading eigenvalues and eigenvectors of large asymmetric matrices, Journal of Scientific Computing 2 (1987) 33–58.
[34] F. Gomez, S. Le Clainche, P. Paredes, M. Hermanns, V. Theofilis, Four decades of studying global linear instability: Progress and challenges, AIAA Journal 50 (2012) 2731–2743.
[35] F. Gómez, P. Paredes, R. Gómez, V. Theofilis, Global stability of cubic and large aspect ratio three-dimensional lid-driven cavities, in: 42nd Fluid Dynamics Conference and Exhibit, New Orleans, LA, June 25–28, 2012, AIAA Paper 2012-3274.
[36] F. Gómez, V. Theofilis, P. Paredes, Q. Liu, H. Wei, On the role of global flow instability analysis in closed loop flow control, in: 42nd Fluid Dynamics Conference and Exhibit, New Orleans, LA, June 25–28, 2012, AIAA Paper 2012-2679.
[37] L.M. Gonzalez, V. Theofilis, R. Gomez-Blanco, Finite element methods for viscous incompressible BiGlobal instability analysis on unstructured meshes, AIAA Journal 45 (2007) 840–854.
[38] L.M. Gonzalez, M. Ahmed, J. Kuehnen, H. Kuhlmann, V. Theofilis, Three-dimensional flow instability in a lid-driven isosceles triangular cavity, Journal of Fluid Mechanics 675 (2011) 369–396.
[39] L.M. Gonzalez, V. Theofilis, S.J. Sherwin, High-order methods for the numerical solution of the biglobal linear stability eigenvalue problem in complex geometries, International Journal for Numerical Methods in Fluids 65 (2011) 923–952.
[40] J. Guermond, G. Migeon, G. Pineau, L. Quartapelle, Start-up flows in a three-dimensional rectangular driven cavity of aspect ratio $1:1:2$ at $Re = 1000$, Journal of Fluid Mechanics 450 (2002) 169–199.
[41] R. Iwatsu, K. Ishii, T. Kawamura, K. Kuwahara, J.M. Hyun, Numerical simulation of three-dimensional flow structure in a driven cavity, Fluid Dynamics Research 5 (1989) 173–189.
[42] R. Iwatsu, J.M. Hyun, K. Kuwahara, Analyses of three-dimensional flow calculations in a driven cavity, Fluid Dynamics Research 6 (1990) 91–102.
[43] C.P. Jackson, A finite-element study of the onset of vortex shedding in flow past variously shaped bodies, Journal of Fluid Mechanics (1987) 23–45.
[44] H. Jasak, Error analysis and estimation for the finite volume method and applications to fluid flows, Ph.D. thesis, Imperial College, 1996.
[45] G. Karniadakis, S.J. Sherwin, Spectral/hp Element for Computational Fluid Dynamics, 2nd edition, Oxford University Press, 2005.
[46] H. Keller, Numerical Solution of Bifurcation and Nonlinear Eigenvalue Problems, Academic Press, 1997.
[47] J. Kim, P. Moin, Application of a fractional-step method to incompressible Navier–Stokes equations, Journal of Computational Physics 59 (1985) 308–323.
[48] D. Knoll, D. Keyes, Jacobian-free Newton–Krylov methods: a survey of approaches and applications, Journal of Computational Physics 193 (2004) 357–397.
[49] J. Koseff, R. Street, Visualisation studies of a shear driven three-dimensional recirculating flow, Journal of Fluids Engineering 106 (1984) 21–29.
[50] J. Koseff, R. Street, The lid-driven cavity flow: A synthesis of qualitative and quantitative observations, Journal of Fluids Engineering 106 (1984) 390–398.
[51] H. Ku, R. Hirsh, T. Taylor, A pseudospectral method for solution of the three-dimensional incompressible Navier–Stokes equations, Journal of Computational Physics 70 (1987) 439–462.
[52] E. Leriche, Direct numerical simulation of a lid-driven cavity flow by a Chebyshev spectral method, Ph.D. thesis, Ecole Polytechnique Federale de Lausanne, 1999.
[53] A. Liberzon, Y. Feldman, A.Y. Gelfgat, Experimental observation of the steady-oscillatory transition in a cubic lid-driven cavity, Physics of Fluids 23 (2011) 23–32.
[54] C.J. Mack, P.J. Schmid, A preconditioned Krylov technique for global hydrodynamic stability analysis of large-scale compressible flows, Journal of Computational Physics 229 (2010) 541–560.

[55] C. Migeon, Details on the start-up development of the Taylor–Gortler-like vortices inside a square-section lid-driven cavity for $1000 < Re < 3200$, Experiments in Fluids 33 (2002) 594–602.
[56] M. Morzyńksi, F. Thiele, Numerical stability analysis of flow about a cylinder, Zeitschrift für Angewandte Mathematik und Mechanik 71 (1991) T424–T428.
[57] R. Natarajan, A. Acrivos, The instability of the steady flow past spheres and disks, Journal of Fluid Mechanics 254 (1993) 323–344.
[58] J.W. Nichols, S. Lele, Global modes and transient response of a cold supersonic jet, Journal of Fluid Mechanics 669 (2011) 225–241.
[59] B. Noack, M. Morzynski, G. Tadmor, Reduced-order Modelling for Flow Control, Springer, Wien, New York, 2011.
[60] P. Paredes, M. Hermanns, S. Le Clainche, V. Theofilis, Order 10^4 speedup in global linear instability analysis using matrix formation, Computer Methods in Applied Mechanics and Engineering 253 (2013) 287–304.
[61] J. Pérez, F. Gómez, R. Gómez, V. Theofilis, A shift-invert strategy for global flow instability analysis using matrix-free methods, in: 42nd Fluid Dynamics Conference and Exhibit, New Orleans, LA, June 25–28, 2012, AIAA Paper 2012-3276.
[62] J. Perez, D. Rodriguez, V. Theofilis, Linear global instability of non-orthogonal incompressible swept attachment-line boundary-layer flow, Journal of Fluid Mechanics 710 (2012) 131–153.
[63] A. Prasad, J. Koseff, Reynols number and end-wall effect on a liddriven cavity flow, Physics of Fluids 1 (1989) 208–218.
[64] N. Ramanan, G. Homsy, Linear stability of liddriven cavity flow, Physics of Fluids 6 (1994) 2690–2701.
[65] P. Roache, Perspective: A method for uniform reporting of grid refinement studies, Journal of Fluids Engineering 116 (1994) 405–413.
[66] D. Rodriguez, V. Theofilis, Massively parallel solution of the BiGlobal eigenvalue problem using dense linear algebra, AIAA Journal 47 (2009) 2449–2459.
[67] Y. Saad, Variations of Arnoldi's method for computing eigenelements of large unsymmetric matrices, Linear Algebra and Its Applications 34 (1980) 269–295.
[68] E. Sanmiguel-Rojas, J. Jimenez-Gonzalez, P. Bohorquez, G. Pawlak, C. Martínez-Bazán, Effect of base cavities on the stability of the wake behind slender blunt-based axisymmetric bodies, Physics of Fluids 23 (2011).
[69] W. Saric, Görtler vortices, Annual Review of Fluid Mechanics 26 (1994) 379–409.
[70] P.N. Shankar, M.D. Deshpande, Fluid mechanics in the driven cavity, Annual Review of Fluid Mechanics 32 (2000) 93–136.
[71] A. Tezuka, Global Stability Analysis of Attached or Separated Flows over a NACA0012 Airfoil, AIAA Paper, 2006-1300, 2006.
[72] A. Tezuka, K. Suzuki, Three-dimensional global linear stability analysis of flow around a spheroid, AIAA Journal 44 (2006) 1697–1708.
[73] V. Theofilis, Globally unstable basic flows in open cavities, AIAA Paper 2000-1965, 2000.
[74] V. Theofilis, On the spatial structure of global linear instabilities and their experimental identification, Aerospace Science and Technology 4 (2000) 249–262.
[75] V. Theofilis, On steady-state flow solutions and their nonparallel global linear instability, in: C. Dopazo (Ed.), Advances in Turbulence VIII, 2000, pp. 35–38.
[76] V. Theofilis, Global linear instability, Annual Review of Fluid Mechanics 43 (2011) 319–352.
[77] V. Theofilis, D. Barkley, S.J. Sherwin, Spectral/hp element technology for flow instability and control, The Aeronautical Journal 106 (2002) 619–625.
[78] V. Theofilis, P.W. Duck, J. Owen, Viscous linear stability analysis of rectangular duct and cavity flows, Journal of Fluid Mechanics 505 (2004) 249–286.
[79] L. Tuckerman, D. Barkley, Bifurcation analysis for timesteppers, in: E. Doedel, L. Tuckerman (Eds.), Numerical Methods for Bifurcation Problems and Large-Scale Dynamical Systems, Springer, Berlin, 2000, pp. 453–566.